Segmentation-inspired Image Registration

Saskia Neuber[1], Pia F. Schulz[1], Sven Kuckertz[2], Jan Modersitzki[1,2]

[1]Institute of Mathematics and Image Computing, University of Lübeck, Germany
[2]Fraunhofer Institute of Digital Medicine, MEVIS, Lübeck, Germany
s.neuber@uni-luebeck.de

Abstract. Artificial intelligence has been used with great success for the segmentation of anatomical structures in medical imaging. We use these achievements to improve classical registration schemes. Particularly, we derive geometrical features such as centroids and principal axes of segments and use those in a combined approach. A smart filtering of the features results in a two phase preregistration, followed in a third phase by an intensity guided registration. We also propose to use a regularization, which enables a coupling of all components of the 3D transformation in a unified framework. Finally, we show how easily our approach can be applied even to challenging 3D medical data.

1 Introduction

Image registration is one of the main tasks in daily clinical routine and is required when for example images of different times have to be compared [1].Inspired by the seminal paper of Wasserthal et. al. [2] we propose a new segmentation based registration procedure. The key idea is that based on a powerful segmentation tool, we generate a set of corresponding features, that is used to initialize the overall registration. Based on the automatically deduced features, we suggest a multi-phase approach similar to [3, 4]. In both approaches [3, 4], it is assumed that corresponding landmarks pairs are available. In a first phase, a starting value is obtained from plain landmark based preregistration. Based on this starting point, an overall energy including an image based similarity measure is minimized in a second phase. In [3] a 2D vector field (VF) regularization [5] and a simple penalty for the landmark match is used. In [4] landmarks are included as a hard constraint and a thin-plate spline (TPS) model for arbitrary dimensions is used for phase one and a curvature regularizer for phase two. In this work, we assume a segmentation, e.g., using the TotalSegmentator (TS) [2] and apply a three-phase procedure. In phase one, we generate landmarks by computing the centroids of segments and include these as a hard constraint in the preregistration. In phase two, we assume the images to be roughly aligned and derive correspondences of additional moment based features, specifically principal axes. Based on this additional information, we continue similarly to phase one. Finally, in phase three, we include an image based similarity term and replace the landmark constraint by an application specific penalty. In all phases, we use the same 3D VF regularizer [6]. To the best of our knowledge this VF regularization has not been used in 3D image registration before. Numerical results on challenging 3D thorax data are presented. Our results highlight the power of this combined approach as well as the advantages and limitations of geometrical features.

A. Maier et al. (Hrsg.), *Bildverarbeitung für die Medizin 2024*,
Informatik aktuell, https://doi.org/10.1007/978-3-658-44037-4_59

2 Material and methods

In this section we first formulate the general registration problem. Thereafter details of the landmark extraction from the segments as well as of the registration phases will be given. Next the procedure is adapted to a specific application, precisely the registration of 3D thorax data. Lastly, we present the experimental data set and the evaluation measures.

2.1 Variational formulation of the registration problem

We briefly recall the general formulation of a registration problem; for details see [1, 7]. Solving a registration problem means minimization of an overall energy J

$$J(y) = D(T[y], R) + S(y) + P(y) \quad \text{subject to} \quad C(y) = 0 \tag{1}$$

where $y : \mathbb{R}^d \to \mathbb{R}^d$ is the wanted transformation, d is the spatial dimension, template T and reference R are functions with compact support in an interval $\Omega \subset \mathbb{R}^d$ and $T[y]$ is the transformed image with $T[y](x) = T(y(x))$ for all x. Moreover D is a potential similarity measure, S is a regularizer, P is a potential penalty, and C is a potential constraint. More details are discussed in the following sections.

Although regularization is in principle arbitrary, we suggest the family

$$S(y; \gamma, W) := \int_W \gamma \|\nabla \operatorname{div} y\|^2 + (1-\gamma)\|\nabla \operatorname{rot} y\|^2 \, dx \tag{2}$$

where either $W = \mathbb{R}^d$ or $W = \Omega$ and $\gamma \in (0, 1)$ balances divergence and curl of the field y. These regularizers perform on complete VF and not only on its components individually [5, 6]. A 2D version and the choice of an optimal parameter γ is discussed in [3]. For our 3D results we use the special case $\gamma = 0.5$, which coincides with the TPS energy as in [4]. However, we use this energy for all phases of the registration. Note, that our approach covers essentially all similarity measures, regularizers and penalty terms and is not limited to a particular setting. For our specific application, we discuss a similarity measure D and a penalty P in Section 2.4.

2.2 Segmentation-based feature extraction

We now discuss the feature generation. Basically, we derive geometrical landmarks from the segments, which we represent as characteristic functions. We assume pairs (τ_j, ρ_j), $j = 1, \ldots, L$ for the segments of the template and reference image. Our procedure is identical for all pairs (τ_j, ρ_j) and therefore we describe it only for one particular pair and omit the index j. Based on moments, we compute centroids c and principal axes v^k [1]. Note that the main axes transformation theorem gives $MV = V\Sigma$, where M is essentially the second order moment matrix, $\Sigma = \operatorname{diag}(\sigma_k^2, k = 1, \ldots, d)$ with $\sigma_j \geq \sigma_{j+1}$ an ordered diagonal matrix of eigenvalues and $V = (v^k, k = 1, \ldots, d)$ the corresponding normalized eigendirection matrix with $\det V = 1$. Besides to the centroids c, we derive potentially $2d$ additional landmarks per segment: $c \pm \sigma_k v^k$, $k = 1, \ldots, d$. However, the computation of the axes is only robust, if the segment has clear orientation, i.e. $\sigma_j \gg \sigma_{j+1}$ for all j. We therefore use the landmarks $c \pm \sigma_k v^k$ only in the latter case

(Fig. 1). For finding correspondences of the additional landmarks based on the principal axes, we assume that after the initial phase (centroids alignment), the main axes of τ and ρ are close to each other. Here we sketch the situation for $d = 2$; the 3D case is along the same lines. Without loss of generality we choose r_A as the first landmark for the principal axes of ρ. Our ordering of the additional landmark is r_A, r_B, r_C, r_D and is motivated by a right handed coordinate system. From the angles $\angle r_A c t_a$ and $\angle r_A c t_b$, we conclude that t_a and not t_b corresponds to r_A. With this ordering the list of landmarks for τ is thus t_a, t_b, t_c, t_d (Fig. 1). We extend the centroid feature list by adding these points.

2.3 Registration Scheme

Following classical landmark registration [1], in the first phase we compute y^{C} as the minimizer of Equation. (1) with $D = 0$, $P = 0$, $S(y) = S(y; \gamma, \mathbb{R}^d)$ and $C(y) = \sum_{j=1}^{L} \|y(r_j) - t_j\|$. Next we compute y^{LM} as minimizer of the same functional, where now the extended feature list derived from the pre-aligned images is used. Note that y^{C} is calculated as an intermediate step to find corresponding landmarks as described in Sec. 2.2, but is discarded as soon as y^{LM} is calculated in the second phase. The intensity based registration performed in the third phase is the minimization of Eq. (1) with $S(y) = \alpha \cdot S(y - y^{\mathrm{LM}}; \gamma, \Omega)$ and $C = 0$. D and P are chosen application specific (Sec. 2.4). Note that the similarity measure is no longer zero and thus we need to introduce a balancing parameter α. Moreover, we only regularize the difference to the preregistration, as this difference can be interpreted as an update of y^{LM}. We restrict the regularization to Ω with Dirichlet boundary condition.

2.4 Application specific parametrization

While the general approach is clearly outlined, it remains to discuss the application depending parametrization and feature extraction. In this paper we focus on the 3D thorax data described in Section 2.5. The output of the TS contains various segments that are not usable in our registration procedure. We exclude all segments that are not fully contained in both images. For the first phase, we bypass the problem of large deformations through breathing motion inside the chest and abdomen by restricting the

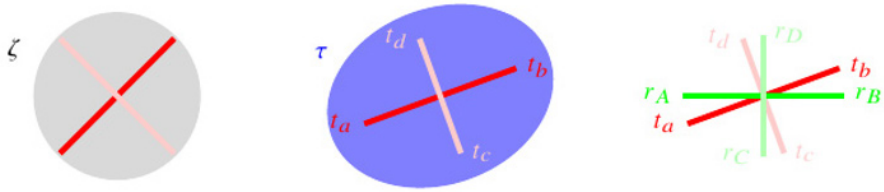

Fig. 1. Visualization of extraction and assignment of additional features. From left to right (main axis: strong, second axis: light): Segment ζ with $\sigma_1 \approx \sigma_2$ (additional features are discarded); segment τ with $\sigma_1 \gg \sigma_2$ and its principal axes; principal axes of τ, ρ after aligning the centroids.

set of centroids to those of rigid structures such as bones. Some segments are visualized in Fig. 2. For the principal axes in the second phase, we only use segments of rigid structures with clear orientation, i.e. $\log_2(\sigma_j/\sigma_{j+1}) > \text{tol}$, where $\text{tol} = 1/3$ is suggested. As similarity measure in the third phase we focus on the classical sum of squared differences restricted to a set $W \subset \Omega$

$$SSD(y; T, R, W) := 1/2 \cdot \|T[y] - R\|^2_{L^2(W)} \tag{3}$$

In particular, we define interior regions of the thorax $\Sigma_T, \Sigma_R \subset \Omega$ using the convex hull of centroids of bone structures (even if they may not be fully contained in both images). Let $\chi_{\Sigma_T}, \chi_{\Sigma_R}$ denote the characteristic functions on these. We assume that after preregistration, the exterior and interior regions roughly align, i.e $\chi_{\Sigma_T}[y^{\text{LM}}] \approx \chi_{\Sigma_R}$, but due to the lung motion not necessarily $T[y^{\text{LM}}] \approx R$ in the interior region. Therefore, we suggest the similarity measure $D(T[y], R) := SSD(y; T, R, \Sigma_R \cap y(\Sigma_T))$, to get a better alignment in the interior region. At the same time we want to keep the alignment of the exterior regions and thus use the penalty $P(y) := \beta \cdot SSD(y; \chi_{\Sigma_T}, \chi_{\Sigma_R}, \Omega)$ with $\beta \in \mathbb{R}_{\geq 0}$.

2.5 Data set

We show results for the publicly available data set [8], which consists of 3D HRCT thorax images with an inspiration and an expiration scan for each subject. We arbitrarily pick case 021 from the test data set and perform the registration between expiration (reference) and inspiration (template). The size of the data is $192 \times 192 \times 208$ voxel each. The TS is used for segmentation followed by the filtering outlined in Sec. 2.4. We obtain eleven bone segments, of which only five provide valid information about the principal axes (Fig. 2). The data set comes with two major challenges, namely large lung motion and a cropped expiration scan.

2.6 Evaluation Measures and Computational Details

The proposed method is evaluated using dice scores for corresponding segments (τ_j, ρ_j) and the energy of the difference image restricted to the thorax region in the reference

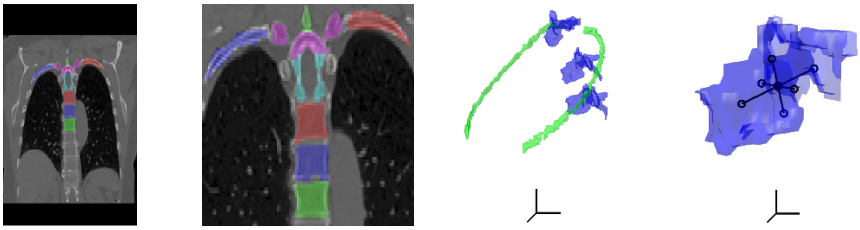

Fig. 2. Visualization of the inspiration scan [8] and bone segments from the TS. From left to right: Coronal slice overlayed with segments; details; 3D view of selected segments (blue and green indicate that only centroids or both, centroids and principal axes are used, respectively); a detailed segment with its centroid and principal axes.

Tab. 1. Mean dices of segments and distances (SSD) in the exterior ($\Gamma \setminus \Sigma_R$) and interior ($\Sigma_R$) of the thorax region ($\Gamma$) before and after registration.

	mean dice of segments in		dist [$\cdot 10^6$] in		
	$\Gamma \setminus \Sigma_R$	Σ_R	$\Gamma \setminus \Sigma_R$	Σ_R	Γ
without registration	0.24	0.51	1.2	5.6	6.9
after preregistration	0.64	0.32	2.0	4.4	6.6
after full registration	0.58	0.61	0.5	4.3	4.9

image $\Gamma \subset \Omega$ or some subset of Γ

$$\text{dice}_j(y) := 2|\tau_j[y] \cap \rho_j|/(|\tau_j[y]| + |\rho_j|) \quad \text{dist}(y) := SSD(y, T, R, \Gamma) \tag{4}$$

In the implementation we use a multilevel approach similar to [4]. The data is interpolated on a 64x64x64 grid, therefore the coarsest level is $l_{\min} = 3$ and the finest level is $l_{\max} = 6$. We set the parameters $\alpha = 500$, $\beta = 10^3$. For the optimization we use a Gauss-Newton scheme and conjugate gradient as solver. All calculations are performed on MATLAB R2022b. Furthermore the FAIR package as described in [7] is used.

3 Results

Next we present numerical results for the 3D thorax data described in Sec. 2.5. Using the parameters from Sec. 2.6 the registration procedure yields transformations y^{LM} and y after preregistration and full registration, respectively. Table 1 summarizes the mean dices of the segments in the interior region $\Sigma_R \subset \Gamma$ and the exterior region $\Gamma \setminus \Sigma_R$ of the thorax region Γ. Additionally the distances in these parts are shown for the different phases of the registration. For the mean dice, we observe that after preregistration it improves considerably on the exterior, whereas it deteriorates in the interior. The latter is due to lung motion and the distribution of landmarks. Therefore, the third phase of our approach focusses on the interior region by adapting the similarity measure and adding a region specific penalty, tolerating a small degradation on the exterior region (Tab. 1). For the distances, we observe an increase on the exterior after preregistration. This is to be expected as this step does not include intensity information. However, the overall approach improves particularly the distance on the thorax region Γ (Tab. 1 and Fig. 3).

4 Discussion

We propose a new segmentation inspired registration procedure. From the automatically derived segments, we extract geometrical features such as centroids and principal axes. These features serve as input for a two-phase landmark based preregistration. Using sensible filtering, the preregistration comprises a rough alignment based on segments of bones in phase one and an extension to principal axes type features in phase two. With this approach, we overcome the difficulty of 3D landmark extraction and in addition provide an outstanding starting value for an intensity based third registration phase.

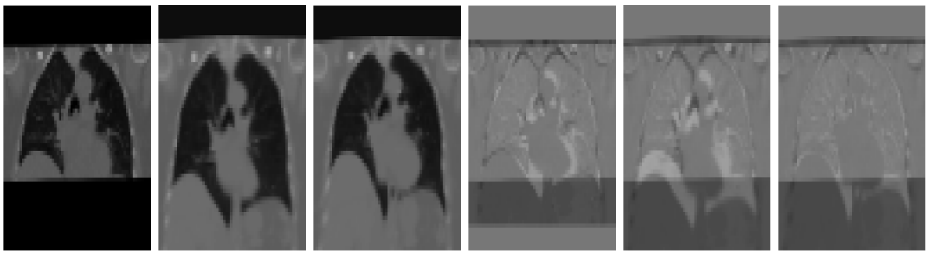

(a) R **(b)** $T(y^{\mathrm{LM}})$ **(c)** $T(y)$ **(d)** $R-T$ **(e)** $R-T(y^{\mathrm{LM}})$ **(f)** $R-T(y)$

Fig. 3. Exemplary selected coronal slices of the 3D thorax images: expiration scan (R); transformed inspiration scan landmark based $T(y^{\mathrm{LM}})$ and final result $T(y)$; and corresponding difference images.

Similarly to [3], we use a vector field regularization energy for all phases. This energy is based on divergence and curl and enables a coupling of all components of the vector field. Note that [3] considers only 2D registration in which the curl is simply a scalar, while we extend to 3D, where the curl becomes a vector field.

A proof of concept is given for challenging 3D thorax data, which show a variety of difficulties including large lung motion and cropped images. We demonstrate that the scheme can easily be adapted to cover also this application, produces impressive results, and reveals the advantages of a hybrid, landmark and intensity based, registration.

In future work, we perform a more comprehensive evaluation on data from different applications. Moreover, we also compare the approach to state-of-the-art alternatives.

References

1. Modersitzki J. Numerical Methods for Image Registration. New York: Oxford University Press, 2004.
2. Wasserthal J, Breit HC, Meyer MT, Pradella M, Hinck D, Sauter AW et al. TotalSegmentator: Robust segmentation of 104 anatomic structures in CT images. Radiol: Artifl Intell. 2023;5(5).
3. Sorzano COS, Thévenaz P, Unser M. Elastic registration of biological images using vector-spline regularization. IEEE Trans Biomedi Engin. 2005;52(4):652–63.
4. Haber E, Heldmann S, Modersitzki J. A scale-space approach to landmark constrained image registration. Proceedings of the Second International Conference on Scale Space Methods and Variational Methods in Computer Vision (SSVM). Springer LNCS, 2009:1–12.
5. Amodei L, Benbourhim M. A vector spline approximation. J Approx Theory. 1991;67(1):51–79.
6. Dodu F, Rabut C. Vectorial interpolation using radial-basis-like functions. Comput & Math Appl. 2002;43(3-5):393–411.
7. Modersitzki J. FAIR: Flexible Algorithms for Image Registration. SIAM, 2009.
8. Hering A, Murphy K, Ginneken B. Lean2Regchallenge: CT lung registration-training data [data set]. 2020.